



Theoretical Analysis of Klinkenberg Correction of Permeability Measurement of Micro/Nanoporous Media

Zhiguo Tian¹ · Mingbao Zhang¹ · Moran Wang¹

Received: 19 March 2024 / Accepted: 18 June 2024
© The Author(s), under exclusive licence to Springer Nature B.V. 2024

Abstract

We present a comprehensive theoretical analysis which integrates the Klinkenberg plot into the pulse decay method (PDM) to effectively address the slippage effect on permeability measurement of micro/nanoporous media. Employing an asymptotic perturbation analysis on the Navier–Stokes equation within a capillary model, our work fills a critical gap in the interpretation of PDM experimental data, particularly by considering the influence of Knudsen number on permeability. Our findings substantiate the reliability of the Klinkenberg plot in interpreting PDM data, particularly when the ratio between the pore volume and the upstream or downstream chamber is below 0.1. It is noteworthy that our study underscores the persistent presence of the slippage effect when one chamber is sealed, emphasizing the necessity for careful consideration in permeability measurements under such conditions. The robustness of the theoretical framework is validated through experimental results, providing strong supports for the accuracy and applicability of our approach in heat and mass studies in micro/nanoporous media.

Keywords Porous media · Permeability · Klinkenberg · Slippage effect · Pulse decay method (PDM)

1 Introduction

Permeability plays a key role in the transport phenomena of porous media (Hughes and Blunt 2000), Landry et al. (2014), Neuzil (2019), Nolte et al. (2021), Zhou et al. (2022), Yuan, et al. (2024). It is a macroscopic physical parameter defined by the Darcy's law and represents the ability of the porous media to let the fluid flow through Philip (1970), Whitaker (1986), Valvatne et al. (2005), Vasseur et al. (2022). The Darcy's law is a linear law, giving the relationship between the pressure gradient and the bulk velocity for steady-state flows and defining the permeability by:

$$-\frac{dP}{dx} = \frac{\mu}{\kappa} v, \quad (1)$$

✉ Moran Wang
mrwang@tsinghua.edu.cn

¹ Department of Engineering Mechanics, Tsinghua University, Beijing 100084, China

where dP/dx is the pressure gradient, μ is the dynamic viscosity of the fluid, v is the bulk velocity, and κ is the permeability.

Accurately quantifying permeability is a fundamental requirement for various applications involving porous media, such as enhanced oil recovery (Doyen (1988)), Suicmez et al. (2007), Akilu et al. (2021), CCUS (Krevor et al. (2015)), Zhang et al. (2020), drug delivery (Prausnitz (1998)), Stoverud et al. (2012), and nuclear waste disposal (Daniels et al. (2017)). Permeability measurement methods typically fall into two categories: steady-state and transient methods (Sander et al. (2017)). The steady-state approach relies on the Darcy's law, maintaining a constant pressure difference between the upper and lower sections to measure the flow rate. However, this method is unsuitable for low-permeability samples due to the time-consuming process of reaching a steady state and challenges in measuring low flow rates. In response, the transient methods, including the pulse decay method (PDM) (Brace et al. (1968)), Hsieh et al. (1981), Neuzil et al. (1981), Trimmer (1981), Kamath et al. (1992), Morrow and Lockner (1994), Jones (1997), Wark and Watson (1998), Cui, et al. (2009), Wang et al. (2021), and the pressure oscillation method (Kranz et al. (1990), Hasanov et al. (2020), were introduced. The pulse decay method has been widely used for its simplicity and accurate representation of in-situ stress conditions. This method involves measuring the pressure change over time by initiating a pressure pulse in the upstream or/and downstream. By describing the flow with the Darcy's law and modeling the transient pressure change through unidirectional mass conservation, a linear governing equation for pressure is derived when the pressure difference is low (Jones (1997)), Cui et al. (2009):

$$\frac{\partial P}{\partial t} = \frac{\kappa_a}{\beta \mu \phi} \frac{\partial^2 P}{\partial x^2}, \quad (2)$$

where κ_a is the apparent permeability, ϕ is the porosity of porous media, and $\beta = \partial \ln \rho / \partial P$ is the gas compressibility. This linear equation, initially formulated by Brace et al. (1968), has been expanded in subsequent studies (Hsieh et al. (1981)), Kamath et al. (1992), Jones (1997), although these expansions are limited to the small pressure difference assumption.

The permeability is an intrinsic property of the porous skeleton, regardless of the fluid type. However, empirical evidence from the prior studies indicates that the measured permeability, commonly referred to as the apparent permeability, tends to exhibit variations with different fluid types. Notably, the slippage effect associated with gas flow, especially when the permeability of the porous material is low and the gas molecule's mean free path is comparable to the mean pore size, is well-acknowledged (Hadjiconstantinou (2024)). Klinkenberg (1941), Moghadam and Chalaturnyk (2014) gave the first model for the slippage effect and the Klinkenberg plot, the apparent permeabilities versus the reciprocal of the mean pressures, has been widely adopted since then to eliminate the slippage effect in the steady-state measurement of permeability:

$$\kappa_a = \kappa_{in} \left(1 + \frac{b}{\bar{P}} \right), \quad (3)$$

where $\bar{P} = (P_u + P_d)/2$ is the arithmetic mean pressure of the upstream and downstream pressure, P_u , P_d ; b is the Klinkenberg factor; κ_{in} is the intrinsic permeability, usually called the Klinkenberg-corrected permeability (Ziarani and Aguilera (2012)). Although concise and applicable in steady-state conditions, the derived form, formula Eq. (3), has limitations when directly applied to the traditional pulse decay method. Combining the formula Eqs. (1), (2) and (3) to eliminate the slippage effect results in a highly nonlinear governing

equation, making it challenging to obtain a concise theoretical solution. Various numerical schemes have been proposed, such as the Jones' assumption of a constant mass flow rate (Jones (1972)) and Wu's scheme based on a constant Klinkenberg factor assumption and history-dependent pressure (Wu and Pruess (1998)). While informative, these approaches lack conciseness and practical applicability in real measurements (Song et al. (2018)). Even more alarming are the experimental findings, revealing a significant deviation between the Klinkenberg-corrected permeability by the Jones's method and the intrinsic permeability, especially notable when dealing with samples of lower permeability—up to ten times larger when intrinsic permeability is $10^{-6} \mu\text{m}^2 (1 \mu\text{m}^2 = 10^{-12} \text{m}^2)$ (Rushing et al. (2004)). Intriguingly, certain experimental work (Nolte et al. (2021)) has demonstrated that directly plotting the Klinkenberg plot in the pulse decay method, measuring the apparent permeabilities by altering mean pressures while maintaining a small pressure difference, yields consistent intrinsic permeability values comparable to the steady-state measurements. However, these experiments lack a detailed explanation of the physical foundation supporting the direct use of the Klinkenberg plot in the pulse decay method.

This study presents a succinct theoretical basis for the Klinkenberg-corrected permeability of microporous media within the traditional pulse decay method, with an emphasis on the small pressure difference assumption. Our work offers a physical rationale for directly employing the Klinkenberg plot to determine intrinsic permeability through the pulse decay method. Additionally, we complement our theoretical framework with experimental validation, confirming the accuracy and reliability of our derived model.

2 Physical and Mathematical Models

The pulse decay method (PDM) apparatus is illustrated in Fig. 1a. The porous sample is considered homogeneous, characterized by the porosity ϕ , extending from location 0 to L . At the initiation of the experiment (time 0), the upstream pressure is lifted, leading to the fluid flow toward the downstream due to the induced pressure difference. The typical pressure–time curve is depicted in Fig. 1b. The late-time solution, applicable in cases of small pressure differences, typically requires that the pressure difference ΔP be less than 10% of the mean pressure \bar{P} , where $\Delta P = P_u - P_d$ (Jones (1997)), Cui et al. (2009).

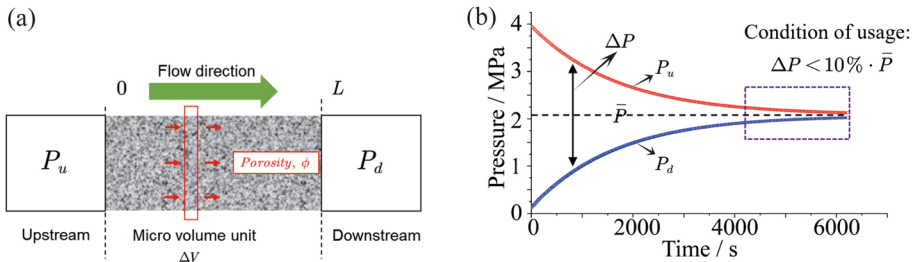


Fig. 1 The apparatus and recorded data of the pulse decay method (PDM): **a** depicts the apparatus. At time 0, the upstream pressure is elevated while the downstream pressure remains constant. **b** Presents a typical pressure–time curve

2.1 Physical Model and Governing Equation

Prior investigations have typically employed the refined form of permeability, expressed as formula Eq. (3), to offer a macroscopic depiction, often overlooking the underlying physical model. In this study, we depart from this trend and utilize the capillarity model to elucidate the pressure pulse decay process, accounting for the slippage effect. Within the capillarity model, our focus narrows down to the governing equation within a single tube, specifically the incompressible Navier–Stokes equation, as outlined in our previous work (Tian et al. (2023)):

$$\bar{\rho} \frac{\partial u_x}{\partial t} = \bar{\mu} \frac{\partial^2 u_x}{\partial x^2} + \bar{\mu} \left(\frac{\partial^2 u_x}{\partial r^2} + \frac{1}{r} \frac{\partial u_x}{\partial r} \right) - \frac{\partial P}{\partial x}, \quad (4)$$

where u_x is the velocity in the flow direction, r is the radial coordinate, x is the flow coordinate, $\bar{\rho}$, $\bar{\mu}$ are the mean density and mean dynamic viscosity of the fluid, respectively. Notably, we exclude the convective term from consideration, as our primary concern lies with cases characterized by small pressure differences.

2.2 Asymptotic Perturbation

Macroscopically, the two forces, that are the viscous force imposed by the fluid flow on the solid boundary of all tubes and the driven force imposed by the pressure gradient on the fluid of all tube, should be balanced. The expressions for these two forces are $\frac{\bar{\mu} \bar{u}}{R} \cdot N \cdot \pi RL$ and $\Delta P(t) \cdot N \pi R^2$, respectively, where \bar{u} is the mean velocity, R is the radius of the tube, N is the number of tubes in capillarity model, and L is the length of the tube. The magnitude of mean velocity can be obtained by equating these two terms, and it is expressed as $\bar{u} \approx \frac{\Delta P(t) R^2}{\bar{\mu} L}$. Then, Eq. (4) can be nondimensionalized by taking:

$$\hat{x} = \frac{x}{L}, \hat{r} = \frac{r}{R}, \hat{u}_z = \frac{u_z}{\bar{u}}, \hat{P} = \frac{P(t)}{\Delta P(0)}, \hat{t} = \frac{R^2 P_u(0)}{\bar{\mu} L^2} t, \quad (5)$$

where the parameter with hat is nondimensionalized, $\Delta P(0)$ is the pressure difference between the upstream and downstream in the initial time $t = 0$, $P_u(0)$ is the initial upstream pressure. And the nondimensionalized form is:

$$\frac{R^4 \bar{\rho} P_u(0)}{(\bar{\mu} L)^2} \frac{\partial \hat{u}_x}{\partial \hat{t}} = \frac{R^2}{L^2} \frac{\partial^2 \hat{u}_x}{\partial \hat{x}^2} + \left(\frac{\partial^2 \hat{u}_x}{\partial \hat{r}^2} + \frac{1}{\hat{r}} \frac{\partial \hat{u}_x}{\partial \hat{r}} \right) - \frac{\Delta P(0) R^2}{\bar{\mu} \bar{u} L} \frac{\partial \hat{P}}{\partial \hat{x}}. \quad (6)$$

After substituting \bar{u} , the magnitude of $\frac{\partial \hat{P}}{\partial \hat{x}}$ is $\frac{\Delta P(0) R^2}{\bar{\mu} L} \approx \frac{\Delta P(0)}{\Delta P(0)} \approx 1$, which depends on the fact that $\Delta P(t)$ is typically chosen at the range of $5\% \cdot \bar{P} \sim 3\% \cdot \bar{P}$ for determining the permeability in experiments. In actual physical process, the transient term $\frac{\partial \hat{u}_x}{\partial \hat{t}}$ is the reason for the velocity change in the flow direction $\frac{\partial^2 \hat{u}_x}{\partial \hat{x}^2}$, which means that these two terms should have the same magnitude, and that gives $\frac{R^4 \bar{\rho} P_u(0)}{(\bar{\mu} L)^2} \approx \frac{R^2}{L^2}$. We combine these two formulas, $\frac{\Delta P(0) R^2}{\bar{\mu} \bar{u} L} \approx 1$ and $\frac{R^4 \bar{\rho} P_u(0)}{(\bar{\mu} L)^2} \approx \frac{R^2}{L^2}$, and obtain $\frac{\Delta P(0)}{P_u(0)} \approx \frac{\bar{\mu} L}{\mu}$. Here, $\frac{\bar{\mu} L}{\mu}$ is the expression for Reynolds number, and it is much smaller than 1, which is consistent with the small pressure

difference constrain, $\frac{\Delta P^{(0)}}{P_v^{(0)}} \simeq \frac{\overline{\rho u L}}{\mu} \ll 1$. Based on these orders of magnitude analysis, the nondimensionalized form with relative magnitudes of each term is:

$$\epsilon^2 \frac{\partial \hat{u}_x}{\partial \hat{t}} = \epsilon^2 \frac{\partial^2 \hat{u}_x}{\partial \hat{x}^2} + \left(\frac{\partial^2 \hat{u}_x}{\partial \hat{r}^2} + \frac{1}{\hat{r}} \frac{\partial \hat{u}_x}{\partial \hat{r}} \right) - \frac{\partial \hat{P}}{\partial \hat{x}}, \tag{7}$$

where $\epsilon = R/L$ is much smaller than 1.

Asymptotic perturbation can be conducted by using ϵ :

$$\hat{u}_x = \hat{u}_x^{(0)} + \epsilon \hat{u}_x^{(1)} + \epsilon^2 \hat{u}_x^{(2)} + \dots, \tag{8}$$

$$\hat{P} = \hat{P}^{(0)} + \epsilon \hat{P}^{(1)} + \epsilon^2 \hat{P}^{(2)} + \dots, \tag{9}$$

where $\hat{u}_x^{(0)}$, $\hat{u}_x^{(1)}$, $\hat{u}_x^{(2)}$ and $\hat{P}^{(0)}$, $\hat{P}^{(1)}$, $\hat{P}^{(2)}$ are independent of ϵ . The forms of asymptotic expansion, formula Eqs. (8) and (9), converges to \hat{u}_x and \hat{P} when ϵ approaches to zero. Then these two expansions, formula Eqs. (8) and (9), are substituted into Eq. (7):

$$\begin{aligned} \mathcal{O}(1) : 0 &= \frac{\partial^2 \hat{u}_x^{(0)}}{\partial \hat{r}^2} + \frac{1}{\hat{r}} \frac{\partial \hat{u}_x^{(0)}}{\partial \hat{r}} - \frac{\partial \hat{P}^{(0)}}{\partial \hat{x}} \\ \mathcal{O}(\epsilon) : 0 &= \frac{\partial^2 \hat{u}_x^{(1)}}{\partial \hat{r}^2} + \frac{1}{\hat{r}} \frac{\partial \hat{u}_x^{(1)}}{\partial \hat{r}} - \frac{\partial \hat{P}^{(1)}}{\partial \hat{x}} \\ \mathcal{O}(\epsilon^2) : \frac{\partial \hat{u}_x^{(0)}}{\partial \hat{t}} &= \frac{\partial^2 \hat{u}_x^{(0)}}{\partial \hat{x}^2} + \left(\frac{\partial^2 \hat{u}_x^{(2)}}{\partial \hat{r}^2} + \frac{1}{\hat{r}} \frac{\partial \hat{u}_x^{(2)}}{\partial \hat{r}} \right) - \frac{\partial \hat{P}^{(2)}}{\partial \hat{x}}, \end{aligned} \tag{10}$$

where the notation $\mathcal{O}(1)$ means that the magnitude of each term in the equation is 1 and $\mathcal{O}(\epsilon)$, $\mathcal{O}(\epsilon^2)$ are the same. Combining the equation of $\mathcal{O}(1)$ with the equation of $\mathcal{O}(\epsilon)$, the equation in the form of $0 = \frac{\partial^2}{\partial \hat{r}^2} [\hat{u}_x^{(0)} + \epsilon \hat{u}_x^{(1)}] + \frac{1}{\hat{r}} \frac{\partial}{\partial \hat{r}} [\hat{u}_x^{(0)} + \epsilon \hat{u}_x^{(1)}] - \frac{\partial}{\partial \hat{x}} [\hat{P}^{(0)} + \epsilon \hat{P}^{(1)}]$ is obtained. It is reasonable to give the form of equation that $0 = \frac{\partial^2 \hat{u}_x}{\partial \hat{r}^2} + \frac{1}{\hat{r}} \frac{\partial \hat{u}_x}{\partial \hat{r}} - \frac{\partial \hat{P}}{\partial \hat{x}}$, which means $0 = \left(\frac{\partial^2 \hat{u}_x^{(2)}}{\partial \hat{r}^2} + \frac{1}{\hat{r}} \frac{\partial \hat{u}_x^{(2)}}{\partial \hat{r}} \right) - \frac{\partial \hat{P}^{(2)}}{\partial \hat{x}}$ and is deduced from Eq. (10). Then, two governing equations in different magnitudes are deduced. In the magnitude of $\mathcal{O}(1)$, the governing equation is:

$$0 = \frac{\partial^2 \hat{u}_x^{(0)}}{\partial \hat{r}^2} + \frac{1}{\hat{r}} \frac{\partial \hat{u}_x^{(0)}}{\partial \hat{r}} - \frac{\partial \hat{P}^{(0)}}{\partial \hat{x}}. \tag{11}$$

In the magnitude of $\mathcal{O}(\epsilon^2)$, the governing equation is:

$$\frac{\partial \hat{u}_x^{(0)}}{\partial \hat{t}} = \frac{\partial^2 \hat{u}_x^{(0)}}{\partial \hat{x}^2}. \tag{12}$$

Equation (11) gives the fluid flow in all circular tubes, which is driven by the pressure gradient, but it only gives the component of $\hat{u}_x^{(0)}(\hat{r}, \hat{x}, \hat{t})$ in the radial direction, \hat{r} . As for Eq. (12), it is caused by the fluid flow from the upstream to the downstream and governs the component of $\hat{u}_x^{(0)}(\hat{r}, \hat{x}, \hat{t})$.

2.3 Analytical and Truncated Solutions

For Eq. (11), its boundary conditions are discussed in the circular tube. To consider the slip-page effect, we introduce a limited value of velocity at the central line and the slip boundary condition on the wall (Klinkenberg (1941)), Lasseux and Valdés-Parada (2017), Battiato et al. (2019):

$$\hat{u}_x^{(0)}|_{\hat{r}=0} \neq \infty, \quad (13)$$

$$\hat{u}_x^{(0)}|_{\hat{r}=1} = -\text{Kn} \left. \frac{\partial \hat{u}_x^{(0)}}{\partial \hat{r}} \right|_{\hat{r}=1}, \quad (14)$$

where Kn is the Knudsen number, $\text{Kn} = \lambda/R$, which is defined as the ratio between the mean free path of the gas molecule λ and the radius of the tube R , ∞ mean infinite value, $\hat{r} = 0$ is the position in the central line of the tube, $\hat{r} = 1$ is the position in the wall of the tube. Formula Eq. (13) means the velocity in the central line of the tube should be a finite value, which is constrained physically. Combining the governing Eq. (11) with its boundary conditions, formula Eqs. (13) and (14), its theoretical solution is:

$$\hat{u}_x^{(0)} = -\frac{1}{4} \frac{\partial \hat{P}^{(0)}}{\partial \hat{x}} (1 - \hat{r}^2 + 2\text{Kn}). \quad (15)$$

The average velocity is then calculated as:

$$\overline{\hat{u}_x^{(0)}} = \frac{\int_0^R u_x \cdot 2\pi r dr}{\pi R^2} = -\frac{1}{8} \frac{\partial \hat{P}^{(0)}}{\partial \hat{x}} (1 + 4\text{Kn}). \quad (16)$$

This average form clearly demonstrates that the velocity changes in the flow direction because the pressure gradient is a transient term, as Fig. 1b demonstrates.

For Eq. (12), its boundary conditions should be introduced in the inlet and outlet. Before doing this, we can substitute formula Eq. (15) into Eq. (12) to obtain the governing equation for pressure since the measured parameter is pressure in experiment. Formula Eq. (15) demonstrates that the velocity is proportional to the pressure gradient and substitution of formula Eq. (15) into Eq. (12) gives $\frac{\partial}{\partial \hat{x}} \left(\frac{\partial \hat{P}^{(0)}}{\partial \hat{t}} - \frac{\partial^2 \hat{u}_x^{(0)}}{\partial \hat{x}^2} \right) = 0$. It is reasonable to choose its trivial solution: $\frac{\partial \hat{P}^{(0)}}{\partial \hat{t}} - \frac{\partial^2 \hat{u}_x^{(0)}}{\partial \hat{x}^2} = 0$. By doing this, Eq. (12) is changed into:

$$\frac{\partial \hat{P}^{(0)}}{\partial \hat{t}} = \frac{\partial^2 \hat{P}^{(0)}}{\partial \hat{x}^2}. \quad (17)$$

After this, we consider the mass conservation in the upstream and downstream chamber to put forward the boundary conditions in the inlet and outlet for Eq. (17). For the upstream chamber, the change rate of mass with time should be equal to the mass flow rate from the upstream chamber to the tubes and this is expressed mathematically as:

$$\frac{\partial(\rho_u V_u)}{\partial t} = - \left(\overline{\hat{\rho} \hat{u}_x^{(0)}} \cdot \bar{u} \right) \Big|_{x=0} N\pi R^2, \quad (18)$$

where ρ_u is the density of the fluid in the upstream chamber, and V_u is the volume of the upstream chamber. Equation (18) is expressed in dimensional form. The left-hand is the change rate of the mass with time in the upstream chamber. The right hand is the mass flow rate from the upstream chamber to the N tubes in the inlet. Substituting the expression for average dimensionless velocity $\overline{\hat{u}_x^{(0)}}$, formula Eq. (16), and that the pressure is linearly proportional to the density, the expression is rewritten as:

$$\frac{\partial \hat{P}^{(0)}}{\partial \hat{t}} = \frac{N\pi R^2 L}{8V_u} \frac{\overline{\mu u} L}{R^2 \Delta P^{(0)}(0)} \frac{\overline{P}^{(0)}}{P_u(0)} \frac{\partial \hat{P}^{(0)}}{\partial \hat{x}} F(\text{Kn}), \tag{19}$$

where $F(\text{Kn}) = 1 + 4\text{Kn}$, $\overline{P}^{(0)} = (P_u^{(0)} + P_d^{(0)})/2$. Due to previous order of magnitude analysis, the magnitudes of $\frac{\overline{\mu u} L}{R^2 \Delta P^{(0)}(0)}$ and $\frac{\overline{P}^{(0)}}{P_u(0)}$ is 1. Therefore, Eq. (19) is simplified as:

$$\left. \frac{\partial \hat{P}^{(0)}}{\partial \hat{t}} \right|_{\hat{x}=0} = \hat{V}_u F(\text{Kn}) \left. \frac{\partial \hat{P}^{(0)}}{\partial \hat{x}} \right|_{\hat{x}=0}, \tag{20}$$

where $\hat{V}_u = \frac{N\pi R^2 L}{8V_u}$ and its physical meaning is 1/8 of the ratio between the pore volume in the measured sample and the volume of the upstream chamber. Similarly, the boundary condition for the outlet is:

$$\left. \frac{\partial \hat{P}^{(0)}}{\partial \hat{t}} \right|_{\hat{x}=1} = -\hat{V}_d F(\text{Kn}) \left. \frac{\partial \hat{P}^{(0)}}{\partial \hat{x}} \right|_{\hat{x}=1}, \tag{21}$$

where $\hat{V}_d = \frac{N\pi R^2 L}{8V_d}$ and its physical meaning is 1/8 of the ratio between the pore volume in the measured sample and the volume of the downstream chamber.

We use the method of separation of variable to solve Eq. (17). The form of the solution is assumed as:

$$\hat{P}^{(0)}(\hat{x}, \hat{t}) = \mathcal{Z}(\hat{x}) \cdot \mathcal{T}(\hat{t}). \tag{22}$$

Substitute the solution form Eq. (22) back into the governing Eq. (17):

$$\frac{\mathcal{Z}''}{\mathcal{Z}} = \frac{\mathcal{T}'}{\mathcal{T}} = -\theta_m^2, \tag{23}$$

where θ_m is a constant, the prime is differential, $\mathcal{Z}'' = \frac{d^2 \mathcal{Z}}{d\hat{x}^2}$ and $\mathcal{T}' = \frac{d\mathcal{T}}{d\hat{t}}$. The ratios, $\frac{\mathcal{Z}''}{\mathcal{Z}}$ and $\frac{\mathcal{T}'}{\mathcal{T}}$, are equal, which is a direct result of the substitution of formula Eq. (22) into Eq. (17). Since $\frac{\mathcal{Z}''}{\mathcal{Z}}$ only depends on \hat{x} and $\frac{\mathcal{T}'}{\mathcal{T}}$ only depends on \hat{t} , the ratios must be constant and the constant is noted as $-\theta_m^2$. Equation (23) represents two separate equations and the corresponding Eigen-functions are:

$$\mathcal{Z} = \mathcal{A} \cdot \sin(\theta_m \hat{x}) + \mathcal{B} \cdot \cos(\theta_m \hat{x}), \tag{24}$$

and

$$\mathcal{T} = \mathcal{C} \cdot e^{-\theta_m^2 \hat{t}}, \tag{25}$$

where \mathcal{A} , \mathcal{B} , \mathcal{C} are constants which need to be determined by the boundary conditions. Substituting the formulas Eq. (24) and Eq. (25) into the boundary conditions, formula Eq. (20) and Eq. (21), these constants are:

$$\mathcal{Z}(0)\mathcal{T}' = \hat{V}_u F(\text{Kn})\mathcal{Z}'(0)\mathcal{T}, \tag{26}$$

$$\mathcal{Z}(1)\mathcal{T}' = -\hat{V}_d F(\text{Kn})\mathcal{Z}'(1)\mathcal{T}, \tag{27}$$

and this gives:

$$\tan \theta_m = \frac{(\hat{V}_u + \hat{V}_d)F(\text{Kn})\theta_m}{\theta_m^2 - \hat{V}_u\hat{V}_dF(\text{Kn})}, \tag{28}$$

$$-\mathcal{B} \cdot \theta_m = \mathcal{A} \cdot \hat{V}_u \cdot F(\text{Kn}). \tag{29}$$

In general, the sum of solutions to Eq. (17) which satisfies the boundary conditions, formula Eqs. (20) and (21), also satisfies Eq. (17). Hence, a complete solution can be given as:

$$\hat{P}^{(0)}(\hat{x}, \hat{t}) = \mathcal{D}_0 + \sum_{m=1}^{\infty} \mathcal{D}_m [\theta_m \sin(\theta_m \hat{x}) - \hat{V}_u F(\text{Kn}) \cdot \cos(\theta_m \hat{x})] e^{-\theta_m^2 \hat{t}}, \tag{30}$$

where the coefficients $\mathcal{D}_m (m = 0, 1, 2, \dots)$ are determined by the initial condition. In actual measurement, the initial condition is expressed in dimensional form as:

$$P(x, 0) = \begin{cases} P_u(0), x = 0 \\ P_d(0), 0 < x \leq L \end{cases}. \tag{31}$$

Now, we return to the asymptotic perturbation form, formula Eq. (9), and rewrite it as:

$$\hat{P} = \hat{P}^{(0)} + \mathcal{O}(\epsilon). \tag{32}$$

This means that the result of \hat{P} can be safely represented by $\hat{P}^{(0)}$, whose error of rounding is on the magnitude of ϵ . Since ϵ is very small, it is safe to say that $\hat{P} = \hat{P}^{(0)}$. Substituting $\hat{t} = 0$ into formula Eq. (30) and letting $\hat{P} = \hat{P}^{(0)}$, the initial condition is:

$$\hat{P}(\hat{x}, 0) = \mathcal{D}_0 + \sum_{m=1}^{\infty} \mathcal{D}_m [\theta_m \sin(\theta_m \hat{x}) - \hat{V}_u F(\text{Kn}) \cdot \cos(\theta_m \hat{x})]. \tag{33}$$

The right hand of formula Eq. (33) is the expansion form of the initial condition by the Eigen-functions. The coefficients, $\mathcal{D}_m (m = 0, 1, 2, \dots)$, can be determined by the orthogonality of the Eigen-functions. Finally, the expression of the solution is:

$$\hat{P}(\hat{x}, \hat{t}) = \mathcal{D}_0 + \sum_{m=1}^{\infty} \mathcal{D}_m [\theta_m \sin(\theta_m \hat{x}) - \hat{V}_u F(\text{Kn}) \cdot \cos(\theta_m \hat{x})] e^{-\theta_m^2 \hat{t}}. \tag{34}$$

In actual measurement, the expression for pressure difference is more practical and it is obtained by substituting $\hat{x} = 0$, $\hat{x} = 1$ and making a subtraction:

$$\Delta \hat{P}(\hat{t}) = \hat{P}(0, \hat{t}) - \hat{P}(1, \hat{t}) = \sum_{m=1}^{\infty} \mathcal{D}_m [\hat{V}_u - \theta_m \sin(\theta_m) + \hat{V}_u F(\text{Kn}) \cos(\theta_m)] e^{-\theta_m^2 \hat{t}}. \tag{35}$$

All the terms ($m \geq 2$) are much smaller than the first term ($m = 1$). We only maintain the first term and that gives:

$$\Delta \hat{P}(\hat{t}) \approx \mathcal{D}_1 [\hat{V}_u - \theta_1 \sin(\theta_1) + \hat{V}_u F(\text{Kn}) \cos(\theta_1)] e^{-\theta_1^2 \hat{t}}. \tag{36}$$

This solution is similar as the previous late-time solution (Brace et al. (1968)), Jones (1997) with seemly a slight difference. Virtually, the main difference lies in the expression for θ_1 . In our solution, after considering the slippage effect, the expression for θ_1 is:

$$\tan \theta_1 = \frac{(\hat{V}_u + \hat{V}_d)F(Kn)\theta_1}{\theta_1^2 - \hat{V}_u \hat{V}_d F(Kn)}, \tag{37}$$

where $F(Kn) = 1 + 4Kn$, θ_1 is the smallest positive solution of Eq. (37).

The dimensional form of formula (36) is:

$$\Delta P(t) = \frac{P_u(t) - P_d(t)}{P_u(0) - P_d(0)} = \mathcal{D}_1 [\hat{V}_u - \theta_1 \sin(\theta_1) + \hat{V}_u F(Kn) \cos(\theta_1)] e^{-\frac{\theta_1^2 R^2 P_u(0)}{\bar{\mu} L^2} t}. \tag{38}$$

After taking logarithm of formula Eq. (38), we can obtain:

$$\ln \Delta P(t) = \mathbb{A} + \mathbb{B}t, \tag{39}$$

where:

$$\mathbb{A} = \ln \{ \mathcal{D}_1 [\hat{V}_u - \theta_1 \sin(\theta_1) + \hat{V}_u F(Kn) \cos(\theta_1)] \}, \tag{40}$$

$$\mathbb{B} = -\frac{\theta_1^2 R^2 P_u(0)}{\bar{\mu} L^2}. \tag{41}$$

The slope \mathbb{B} can be obtained by fitting the experimental data, the recorded pressure difference $\ln \Delta P(t)$ versus the time t . Finally, the permeability expression in capillary model is $\kappa = \frac{\phi R^2}{8}$ and is written as:

$$\kappa = \frac{-\mathbb{B} \bar{\mu} \phi L^2}{8 \theta_1^2 P_u(0)}, \tag{42}$$

where \mathbb{B} is the slope of the fitting line, Eq. (39), in which $\Delta P(t) = \frac{P_u(t) - P_d(t)}{P_u(0) - P_d(0)}$, θ_1 is the smallest positive solution of the transcendental Eq. (37).

2.4 Derivation of Klinkenberg Plot

Then, we show how to eliminate the slippage effect in traditional pulse decay method. In traditional late-time solution without considering the slippage effect, the derivation process is similar as the process shown above and the key difference lies in the boundary condition, formula Eq. (14). Without taking the slippage effect into account, the no-slip boundary condition is used:

$$\hat{u}_x^{(0)}|_{\hat{r}=1} = 0, \tag{43}$$

and the other processes are totally the same as the processes above. The different results mainly lie in the expression for θ_1 , κ , and we note them as θ'_1 , κ' for case without slippage effect. The expression for θ'_1 is:

$$\tan \theta'_1 = \frac{(\hat{V}_u + \hat{V}_d)\theta'_1}{\theta_1'^2 - \hat{V}_u \hat{V}_d}. \tag{44}$$

θ'_1 is the smallest positive solution of Eq. (44). This difference is the key for interpreting the experimental data by considering the slippage effect in the pulse decay method. The expression for κ' is:

$$\kappa' = \frac{-\mathbb{B}\bar{\mu}\phi L^2}{8\theta_1^2 P_u(0)}. \tag{45}$$

In the conditions that \hat{V}_u, \hat{V}_d are much smaller than 1, the magnitudes and relationships can be assumed as:

$$\hat{V}_u, \hat{V}_d \ll \theta_1, \theta'_1 \ll 1. \tag{46}$$

$\theta_1 \approx \tan \theta_1, \theta'_1 \approx \tan \theta'_1$ can be obtained. Besides, the magnitude of $F(\text{Kn}) = 1 + 4\text{Kn}$ is $\mathcal{O}(1)$. Combining Eq. (37), (44) and the relationship Eq. (46), the ratio between θ_1 and θ'_1 is:

$$\frac{\theta_1^2}{\theta_1'^2} \approx F(\text{Kn}) = 1 + 4\text{Kn}. \tag{47}$$

Substituting formula (47) into formula Eqs. (42) and (45), the relationship between the intrinsic permeability κ and the apparent permeability κ' is expressed as:

$$\kappa' = \kappa(1 + 4\text{Kn}). \tag{48}$$

Here, according to the kinetic theory, λ is linearly proportional to the reciprocal of the mean pressure \bar{P} . The relationship between the apparent permeability κ' and the mean pressure \bar{P} is finally:

$$\kappa' = \kappa \left(1 + \frac{b'}{\bar{P}} \right), \tag{49}$$

where b' is a constant, κ' is the apparent permeability directly given by the traditional late-time solution, Eq. (45), κ is the intrinsic permeability and also the intercept of the linear line. It is easy to see that Eq. (49) is the same as Eq. (3). The difference is that Eq. (49) is used for the measurement results of pulse decay method and derived by some assumptions, formula Eq. (46), while Eq. (3) is used for steady-state measurement. The assumption, formula Eq. (46), should be carefully discussed to give the theoretical scope of application in actual measurement. Next, we discuss the theoretical scope of applying Eq. (49) in experimental measurement.

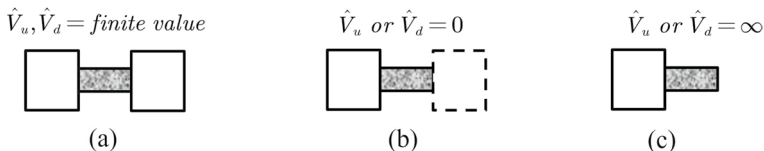


Fig. 2 The various experimental setups primarily emphasizing the volumes of the chambers. **a** Both the upstream and downstream chamber volumes are finite, resulting in finite values for the ratios \hat{V}_u and \hat{V}_d . **b** One of the chamber volumes is infinite, rendering either \hat{V}_u or \hat{V}_d equal to 0. **c** One of the chamber volumes is 0, leading to a scenario where either \hat{V}_u or \hat{V}_d is infinite, ∞

2.5 Theoretical Scope of Application

The previous mentioned assumption, formula Eq. (46), is mainly controlled by the values of \hat{V}_u and \hat{V}_d , whose meanings are 1/8 of the ratios between the pore volume in the measured sample and the volumes of the upstream and downstream chambers, respectively, as shown in Fig. 2. We discuss the theoretical scopes of application in different cases (Wang et al. (2021)).

2.5.1 $\hat{V}_u, \hat{V}_d = \text{Finite Value}$

When the volumes of the upstream and downstream chambers are finite values, the ratios, \hat{V}_u , and \hat{V}_d , are also finite values. Without loss of generality, we let $\hat{V}_u = \hat{V}_d$. Eq. (44) is numerically solved by different values of \hat{V}_u , and the results are demonstrated as Fig. 3a. We only show the results for Eq. (44) because the solutions of Eq. (37) are close to Eq. (44) since the value of $F(Kn)$ is much close to 1 and also Eq. (37) is impossibly difficult to be solved without actual experimental data. As Fig. 3a shows, when \hat{V}_u is smaller than 0.02, the ratio θ'_1/\hat{V}_u is larger than 10 and the ratio $\theta'_1/\tan\theta'_1$ is larger than 0.987. That means that when \hat{v}_u is smaller than 0.02, our assumption, formula Eq. (46), is safe to use and Eq. (49) is true.

2.5.2 \hat{V}_u or $\hat{V}_d = 0$

Then, we consider one of the upstream, and downstream chambers are infinitely large. Without loss of generality, we let $\hat{V}_d = 0$. The results are shown in Fig. 3b. When \hat{V}_u is smaller than 0.01, the ratio θ'_1/\hat{V}_u is larger than 10 and the ratio $\theta'_1/\tan\theta'_1$ is larger than 0.997. That means that when \hat{v}_u is smaller than 0.01, formula Eq. (46) is safe to use and Eq. (49) is true.

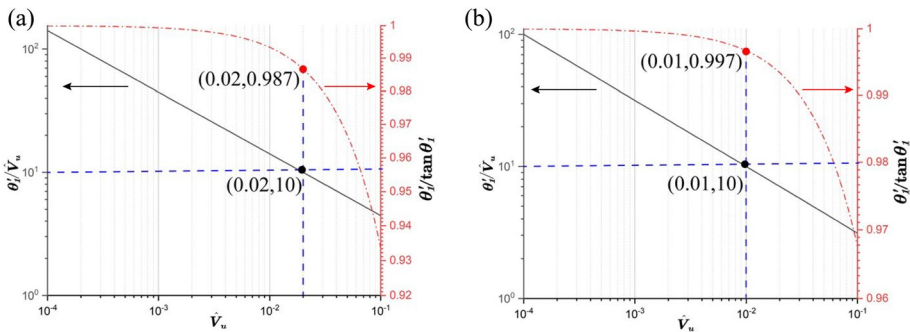


Fig. 3 The ratios, θ'_1/\hat{V}_u and $\theta'_1/\tan\theta'_1$, changes with \hat{V}_u as numerical solutions of Eq. (44) by assigning different values of \hat{V}_u when **a** $\hat{V}_u = \hat{V}_d = \text{finite value}$; **b** $\hat{V}_d = 0$

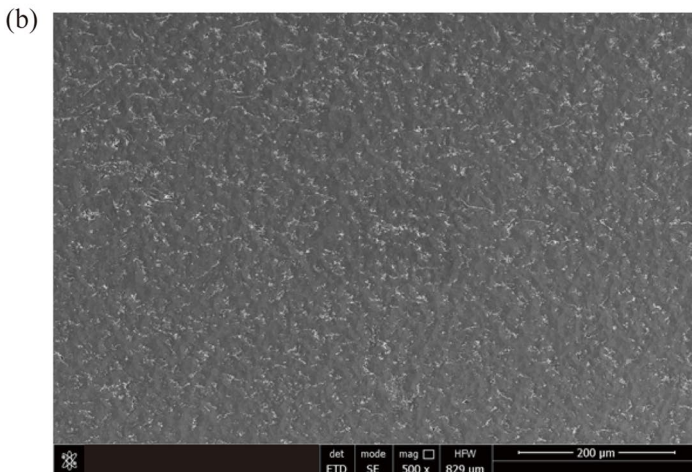
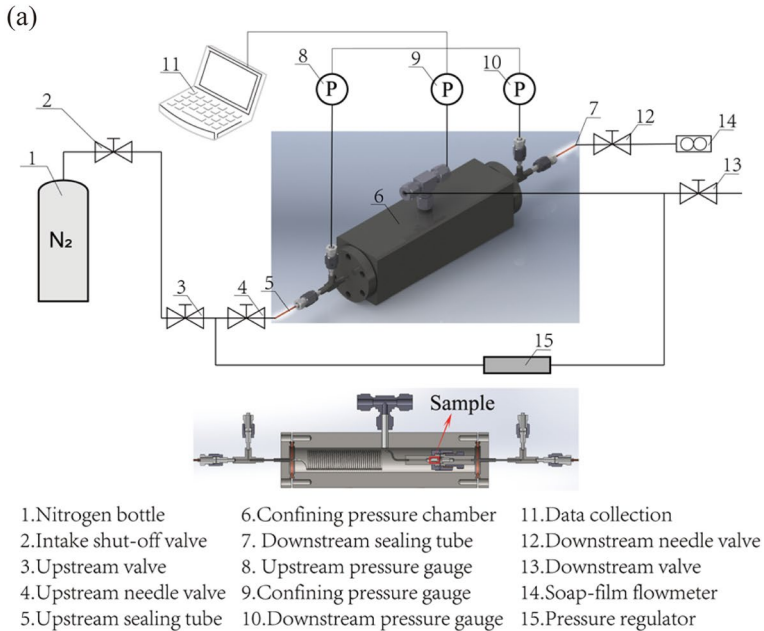


Fig. 4 **a** The diagram of experimental platform. Sample is put in the confining pressure chamber, whose profile is shown below. The highlight of our setup lies in that the measurements using pulse decay method and steady-state method can be conducted by the same platform. The pulse decay method can be conducted by sealing the upstream or downstream sealing tubes, noted as 5 and 7, and forming the upstream and downstream chambers. The steady-state measurement can be conducted by opening the downstream needle valve and linking the soap-film flowmeter for measuring the flow rate. **b** The scanning electron microscopy (SEM) image of the sample

Table 1 The physical parameters of the measured samples

Sample	Porosity	Radius/mm	Length/mm	Intrinsic permeability, PDM/ $10^{(-6)}\mu\text{m}^2$	Intrinsic permeability, steady state/ $10^{(-6)}\mu\text{m}^2$	Relative error
1	7.50%	1.10	6.50	7.01	7.29	3.84%
2	7.50%	1.10	6.50	1.59	1.72	7.56%

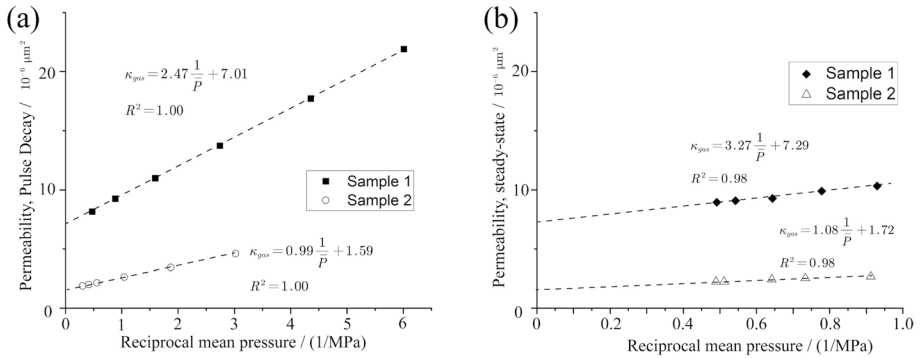


Fig. 5 The measurement results for two samples and the fitting lines are given: **a** the Klinkenberg plots using the apparent permeabilities by pulse decay method. **b** The Klinkenberg plots using the measurements of steady-state method

2.5.3 \hat{V}_u or $\hat{V}_d = \infty$

The last case is when one of the upstream or downstream chambers is zero, which means \hat{V}_u or \hat{V}_d is infinitely large. In this case, formula Eq. (46) cannot be true. Based on analysis above, we conclude that when \hat{V}_u or \hat{V}_d are smaller than 0.01, the direct usage of Klinkenberg plot, the apparent permeability obtained by pulse decay method versus the mean pressure, is always safe in the pulse decay method. We should point out \hat{V}_u or \hat{V}_d are defined as 1/8 of the ratios between the pore volume of the porous media and the volumes of the upstream and downstream chambers, respectively. Roughly speaking, when the pore volume of the measured porous media is larger than 0.1 of volumes of the upstream and downstream chambers, our theoretical derivation is true.

3 Experimental Validation

To verify our theoretical derivation, we set up an experimental platform as Fig. 4 shows. This setup is produced by machining, and its machining and milling accuracy are IT7, graded by National Standards of the People’s Republic of China (coded as GB). The volumes of all tubes are precisely controlled and the volumes of the upstream and downstream chambers, including the tubes and the empty volumes of the pressure gauge, after sealing the upstream and downstream sealing tubes, are measured by lifting the pressure

of one chamber and waiting for the equilibrium. The volumes of the upstream and downstream chambers are 1428.68 mm^3 and 1498.80 mm^3 , respectively. Both the pulse decay method and the steady-state method can be conducted by using this platform. When conducting the pulse decay method, the upstream pressure is lifted by the high-pressure Nitrogen bottle and the sealing tubes, noted as 5 and 7 in Fig. 4, are closed. In this way, an isolated volume is constructed and the gas flows through the sample to the downstream. When conducting the steady-state method, all valves are open and a constant pressure difference is established between the upstream and the downstream. The soap-film flowmeter is used for measuring the low flow rate, whose best precision can be as low as $5 \text{ }\mu\text{L}$. The steady-state measurement is used as the benchmark. The system is carefully leak-tested. The smallest permeability that our platform can measure is $10^{-10} \text{ }\mu\text{m}^2$, which is estimated by the largest leak rate. Our sample is cylindrical, whose radius and length are 1.10 mm and 6.50 mm , respectively. Before measurement, the porosities of tested samples are measured by Mercury Porometer, as Table 1 shows.

The measurement results are presented in Fig. 5 for two samples, with their porosities determined using a Mercury Porometer and recorded as 7.50%, as detailed in Table 1. Utilizing the measured porosities, precise calculations yield values for parameters \hat{V}_u or \hat{V}_d , falling within the magnitude of 10^{-4} and aligning with the theoretical scope of application discussed previously. Then, we measure their permeabilities using the pulse decay method and steady-state method. For each set of measurements, mean pressures are varied, apparent permeabilities are obtained, and Klinkenberg plots are constructed. Figure 5a is the Klinkenberg plots using the apparent permeabilities by pulse decay method. In these measurements, the initial upstream pressure is elevated, and late-time data, where the upstream pressure is more than 10% of the downstream pressure, is utilized to calculate apparent permeabilities using Eq. (45). Figure 5b illustrates the Klinkenberg plots derived from steady-state method measurements. In this method, the downstream pressure remains at atmospheric pressure, while the upstream pressure is varied to obtain different apparent permeabilities at various mean pressures. The fitting lines and correlation coefficients are provided for both methods, demonstrating a high linearity between apparent permeabilities and mean pressures, with coefficients of correlation not less than 0.98. The intercepts are the intrinsic permeabilities. Finally, intrinsic permeabilities obtained through both methods are compared in Table 1, with relative errors of 3.84% and 7.56%, respectively, affirming the accuracy and validity of our theoretical derivation.

4 Conclusion

In this work, we present a thorough theoretical derivation process for the direct utilization of the Klinkenberg plot in the traditional pulse decay method, effectively bridging theoretical gaps evident in prior research and establishing a robust foundation for experimental measurements. Our results demonstrate the reliability, particularly when the ratio between the pore volume of porous media and the upstream or downstream chambers is less than 0.1. Notably, we emphasize that when one of the upstream and downstream chambers is sealed, the persistence of the slippage effect necessitates scrutiny of measured permeability, cautioning against the potential inaccuracies. This insight contributes to a more nuanced understanding of its applicability and underscores the importance of considering experimental conditions for accurate permeability assessments.

Acknowledgements This work is financially supported by the NSF grant of China (No. U1837602), the National Key R&D Program of China (No. 2019YFA0708704) and the Tsinghua University Initiative Scientific Research Program.

Funding National Natural Science Foundation of China, U1837602, Moran Wang

Declarations

Conflict of interest There is no conflict of interests.

References

- Akilu, S., Padmanabhan, E., Sun, Z.: A review of transport mechanisms and models for unconventional tight shale gas reservoir systems. *Int. J. Heat Mass Transf.* **175**, 121125 (2021)
- Battiatto, I., O'Malley, D., Miller, C.T., Takhar, P.S., Valdés-Parada, F.J., Wood, B.D.: Theory and applications of macroscale models in porous media. *Transp. Porous Media* **130**(1), 5–76 (2019)
- Brace, W.F., Walsh, J.B., Frangos, W.T.: Permeability of granite under high pressure. *J. Geophys. Res.* **73**(6), 2225–2236 (1968)
- Cui, X., Bustin, A., Bustin, R.M.: Measurements of gas permeability and diffusivity of tight reservoir rocks: different approaches and their applications. *Geofluids* **9**(3), 208–223 (2009)
- Daniels, K.A., Harrington, J.F., Zihms, S.G., Wiseall, A.C.: Bentonite permeability at elevated temperature. *Geosciences* **7**(1), 3 (2017)
- Doyen, P.M.: Permeability, conductivity, and pore geometry of sandstone. *J. Geophys. Res.: Sol. Earth* **93**(B7), 7729–7740 (1988)
- Hadjiconstantinou, N.G.: Molecular Mechanics of Liquid and Gas Slip Flow. *Annu. Rev. Fluid Mech.* **56**(1), 435–461 (2024)
- Hasanov, A.K., Dugan B., Batzle, M.L.: Numerical simulation of oscillating pore pressure experiments and inversion for permeability. *Water Resour. Res.* **56**(6), e2019WR025681 (2020)
- Hsieh, P.A., Tracy, J.V., Neuzil, C.E., Bredehoeft, J.D., Silliman, S.E.: A transient laboratory method for determining the hydraulic properties of 'tight' rocks—I theory. *Int. J. Rock Mech. Min. Sci. Geomech. Abstr.* **18**, 245 (1981)
- Hughes, R.G., Blunt, M.J.: Pore scale modeling of rate effects in imbibition. *Transp. Porous Media* **40**(3), 295–322 (2000)
- Jones, S.C.: A rapid accurate unsteady-state Klinkenberg permeameter. *Soc. Petrol. Eng. J.* **12**(05), 383–397 (1972)
- Jones, S.C.: A technique for faster pulse-decay permeability measurements in tight rocks. *SPE Form. Eval.* **12**(01), 19–26 (1997)
- Kamath, J., Boyer, R.E., Nakagawa, F.M.: Characterization of core-scale heterogeneities using laboratory pressure transients. *SPE Form. Eval.* **7**(03), 219–227 (1992)
- Klinkenberg, L.J.: The permeability of porous media to liquids and gases. *Drill. Prod. Pract.* **2**, 200–213 (1941)
- Kranz, R.L., Saltzman, J.S., Blacic, J.D.: Hydraulic diffusivity measurements on laboratory rock samples using an oscillating pore pressure method. *Int. J. Rock Mech. Min. Sci. Geomech. Abstr.* **27**, 345 (1990)
- Krevor, S., Blunt, M.J., Benson, S.M., Pentland, C.H., Reynolds, C., Al-Menhali, A., Niu, B.: Capillary trapping for geologic carbon dioxide storage—from pore scale physics to field scale implications. *Int. J. Greenh. Gas Control* **40**, 221–237 (2015)
- Landry, C., Karpyn, Z., Ayala, O.: Relative permeability of homogenous-wet and mixed-wet porous media as determined by pore-scale lattice Boltzmann modeling. *Water Resour. Res.* **50**(5), 3672–3689 (2014)
- Lasseux, D., Valdés-Parada, F.J.: On the developments of Darcy's law to include inertial and slip effects. *Comptes Rendus. Mécanique* **345**(9), 660–669 (2017)
- Moghadam, A.A., Chalaturnyk, R.: Expansion of the Klinkenberg's slippage equation to low permeability porous media. *Int. J. Coal Geol.* **123**, 2–9 (2014)
- Morrow, C.A., Lockner, D.A.: Permeability differences between surface-derived and deep drillhole core samples. *Geophys. Res. Lett.* **21**(19), 2151–2154 (1994)
- Neuzil, C.: Permeability of clays and shales. *Annu. Rev. Earth Planet. Sci.* **47**, 247–273 (2019)
- Neuzil, C.E., Cooley, C., Silliman, S.E., Bredehoeft, J.D., Hsieh, P.A.: A transient laboratory method for determining the hydraulic properties of 'tight' rocks—II. Application. *Int. J. Rock Mech. Min. Sci. Geomech. Abstr.* **18**(3), 253–258, Pergamon. (1981)

- Nolte, S., Fink, R., Krooss, B.M., Amann-Hildenbrand, A., Wang, Y., Wang, M., Schmatz, J., Klaver, J., Littke, R.: Experimental investigation of gas dynamic effects using nanoporous synthetic materials as tight rock analogues. *Transp. Porous Media* **137**(3), 519–553 (2021)
- Philip, J.R.: Flow in Porous Media. *Annu. Rev. Fluid Mech.* **2**(1), 177–204 (1970)
- Prausnitz, M.R., Noonan, J.S.: Permeability of cornea, sclera, and conjunctiva: a literature analysis for drug delivery to the eye. *J. Pharm. Sci.* **87**(12), 1479–1488 (1998)
- Rushing, J., Newsham, K., Lasswell, P., Cox, J., Blasingame, T.: Klinkenberg-corrected permeability measurements in tight gas sands: steady-state versus unsteady-state techniques. In: *SPE Annual Technical Conference and Exhibition*, OnePetro, (2004)
- Sander, R., Pan, Z., Connell, L.D.: Laboratory measurement of low permeability unconventional gas reservoir rocks: A review of experimental methods. *J. Nat. Gas Sci. Eng.* **37**, 248–279 (2017)
- Song, W., Yao, J., Ma, J., Li, Y., Han, W.: A pore structure based real gas transport model to determine gas permeability in nanoporous shale. *Int. J. Heat Mass Transf.* **126**, 151–160 (2018)
- Stoverud, K.H., Darcis, M., Helmig, R., Hassanizadeh, S.M.: Modeling concentration distribution and deformation during convection-enhanced drug delivery into brain tissue. *Transp. Porous Media* **92**(1), 119–143 (2012)
- Suicmez, V.S., Piri, M., Blunt, M.J.: Pore-scale simulation of water alternate gas injection. *Transp. Porous Media* **66**(3), 259–286 (2007)
- Tian, Z., Zhang, D., Wang, Y., Zhou, G., Zhang, S., Wang, M.: Inertial solution for high-pressure-difference pulse-decay measurement through microporous media. *J. Fluid Mech.* **971**, R1 (2023)
- Trimmer, D.A.: Design criteria for laboratory measurements of low permeability rocks. *Geophys. Res. Lett.* **8**(9), 973–975 (1981)
- Valvatne, P.H., Piri, M., Lopez, X., Blunt, M.J.: Predictive pore-scale modeling of single and multiphase flow. *Transp. Porous Media* **58**(1–2), 23–41 (2005)
- Vasseur, J., Wadsworth, F.B., Bretagne, E., Dingwell, D.B.: Universal scaling for the permeability of random packs of overlapping and nonoverlapping particles. *Phys. Rev. E* **105**(4), L043301 (2022)
- Wang, Y., Tian, Z., Nolte, S., Amann-Hildenbrand, A., Krooss, B.M., Wang, M.: Reassessment of transient permeability measurement for tight rocks: The role of boundary and initial conditions. *J. Nat. Gas Sci. Eng.* **95**, 104173 (2021)
- Wark, D.A., Watson, E.B.: Grain-scale permeabilities of texturally equilibrated, monomineralic rocks. *Earth Planet. Sci. Lett.* **164**(3–4), 591–605 (1998)
- Whitaker, S.: Flow in porous media I: A theoretical derivation of Darcy's law. *Transp. Porous Media* **1**(1), 3–25 (1986)
- Wu, Y.-S., Pruess, K.: Gas flow in porous media with Klinkenberg effects. *Transp. Porous Media* **32**(1), 117–137 (1998)
- Yuan, L., Zhang, Y., Liu, S., Zhang, Y., Chen, C., Song, Y.: Study on the slip behavior of CO₂-crude oil on nanopore surfaces with different wettability. *Int. J. Heat Mass Transf.* **218**, 124787 (2024)
- Zhang, Z.T., Wang, M.J., Blunt, E.J., Anthony, A.-H., Park, A., Hughes, R.W., Webley, P.A., Yan, J.: Advances in carbon capture, utilization and storage. *Appl. Energy* **278**, 1156275 (2020)
- Zhou, W., Yang, X., Liu, X.: Multiscale modeling of gas flow behaviors in nanoporous shale matrix considering multiple transport mechanisms. *Phys. Rev. E* **105**(5), 055308 (2022)
- Ziarani, A.S., Aguilera, R.: Knudsen's permeability correction for tight porous media. *Transp. Porous Media* **91**(1), 239–260 (2012)

Publisher's Note Springer Nature remains neutral with regard to jurisdictional claims in published maps and institutional affiliations.

Springer Nature or its licensor (e.g. a society or other partner) holds exclusive rights to this article under a publishing agreement with the author(s) or other rightsholder(s); author self-archiving of the accepted manuscript version of this article is solely governed by the terms of such publishing agreement and applicable law.